Temporal stability of network partitions

Giovanni Petri[1,*] and Paul Expert[2]

[1]*ISI Foundation, Via Alassio 11/c, 10126 Turin, Italy*

[2]*Centre for Neuroimaging Sciences, Institute of Psychiatry, De Crespigny Park, King's College London, London SE5 8AF, United Kingdom*

(Received 19 November 2013; revised manuscript received 17 July 2014; published 25 August 2014)

We present a method to find the best temporal partition at any time scale and rank the relevance of partitions found at different time scales. This method is based on random walkers coevolving with the network and as such constitutes a generalization of partition stability to the case of temporal networks. We show that, when applied to a toy model and real data sets, temporal stability uncovers structures that are persistent over meaningful time scales as well as important isolated events, making it an effective tool to study both abrupt changes and gradual evolution of a network mesoscopic structures.

DOI: 10.1103/PhysRevE.90.022813 PACS number(s): 89.75.Fb, 89.75.Hc

I. INTRODUCTION

Identifying mesoscopic structures and their relation to the function of a system in biological, social, and infrastructural networks is one of the main challenges for complex network analysis [1]. Until recently, most approaches focused on static network representations, although most systems of interests are inherently dynamical [2]. Recent theoretical progress and the availability of data inspired a few innovative methods, which mostly revolve around unfolded static representations of a temporal dynamics [3,4], constraints on the community structure of consecutive graph snapshots [5,6], or global approaches [7–11].

In this article we take a different route and tackle the problem of finding and characterizing the relevance of community structures at different time scales by directly incorporating the time dependence in the method. Inspired by the notion of stability [12], we propose a related measure, *temporal stability*, which naturally embeds the time dependence and order of interactions between the constituents of the system. Temporal stability allows us not only to compare the goodness of partitions over specific time scales, as its static counterpart, but also to find the best partition at any time and over any time scale. In the following we briefly review the main ingredients of static stability and introduce their natural extensions to temporal networks. We then present a benchmark model as a proof of principle and then analyze two real-world data sets, finding pertinent mesoscopic structures at different time scales.

II. TEMPORAL STABILITY

Like the map equation [13,14], stability exploits the properties of the stationary distribution random walkers exploring a static network and of long persistent flows on a network. While the map equation relies on finding the most compressed description of a random walker trajectory in terms of its asymptotic distribution, the intuition behind stability is that walkers exploring the network will tend to stay longer in a well defined cluster before escaping to explore the rest of the network. The object of interest is thus the autocovariance matrix of an unbiased random walk on a network G for a given partition $\mathscr{H}$, i.e., the higher the autocorrelation, the better the description of a system in terms of modules by $\mathscr{H}$. After τ Markov time steps of exploration of the network by the random walkers, it can be compactly written as

$$R_\tau = \mathbf{H}^T\left(\Pi \mathbf{M}_G^\tau - \pi^T\pi\right)\mathbf{H}, \tag{1}$$

where $\mathbf{H}$ is the partition matrix assigning nodes to communities, $\mathbf{M_G}$ is the transition matrix of the random walk on G, π is its stationary distribution, and $\Pi = \mathrm{diag}(\pi)$ [12]. The $\pi^T\pi$ term can be interpreted as a null model that represents the asymptotic modular structure against which the structure unveiled by the random walkers' exploration of the network is tested. The stability of partition $\mathscr{H}$ at Markov time τ is then defined by

$$r_{\mathscr{H}} = \min_{0\leqslant s<\tau} \mathrm{Tr}\, R_s. \tag{2}$$

The magnitude of the trace of the autocovariance matrix represents the extent to which walkers are confined within the clusters defined by $\mathscr{H}$. The minimum over the Markov time during which the walkers were allowed to move ensures that the measure is conservative. The value of τ at which a given partition becomes optimal conveys information about which topological scales of the network are best described by the partition considered. Moreover, the interval over which a partition is optimal is related to the importance of that specific scale across the hierarchy of scales present in the network. Extending this measure to temporal networks requires generalizing its ingredients: the partition $\mathscr{H}$, the transition matrix M_G, and the asymptotic walker distribution π.

Temporal partition. Let us define a discrete temporal network $G\{t\}$ as a time-ordered collection of graph snapshots $G\{t\} = \{G_0, G_1, \ldots, G_T\}$ represented by their adjacency matrices $\{\mathbf{A}_0, \mathbf{A}_1, \ldots, \mathbf{A}_T\}$. The static partition matrix is naturally extended to the temporal case by allowing it to be time dependent, $\mathscr{H} \to \mathscr{H}\{t\} = \{\mathbf{H}(t) | t = 0, 1, \ldots, T\}$, with T the number of slices in the temporal data set. At this point it is worth noting that $\mathscr{H}\{t\}$, like $G\{t\}$, does not need to change at every time step.

Transition matrix. The transition matrix $\mathbf{M}$ will in general change between time steps and therefore one does not simply iterate it. We define $\mathbf{M}_t$, the single-snapshot transition matrix relative to G_t, as $\mathbf{M}_t = \lim_{\epsilon\to 0}(\mathbf{D_t})^{-1}(\epsilon\mathbb{1} + \mathbf{A}_t)$, with $\mathbf{D}_t = (\epsilon\mathbb{1} + \mathbf{A}_t)\cdot\mathbf{1}$, where $\mathbf{1}$ is the constant vector with unit

*giovanni.petri@isi.it

components. The ϵ limit is equivalent to including a self-loop of vanishing weight and is required to ensure that the transition matrix is well defined for nodes that are disconnected at time t.[1] Using the matrices M_t, we can define a time-ordered product $\mathcal{M}_G(t,\tau)$ that represents the transition matrix for the evolution of the random walker across the changing network between t and $t+\tau$:

$$\mathcal{M}_G(t,\tau) = \mathcal{T}\{\mathbf{M}_t,\ldots,\mathbf{M}_{t+\tau}\} = \prod_{s=t}^{t+\tau}\mathbf{M}_s = \mathbf{M}_{t+\tau}\cdots\mathbf{M}_t, \tag{3}$$

where we impose right multiplication to respect the arrow of time.

Stationary walker distribution. The last element we need is the stationary walker distribution on a time-varying network. We will denote this distribution by ω. Different types of random walks can be devised, depending on the model for the dynamics of the network; therefore ω is not unique: Different dynamics preserve different statistical features of the system. Here we consider the case where the time-evolving connectivity of each node is known. The activity-driven model, introduced by Perra *et al.* [15], is particularly adapted to such systems. It provides a null model akin to a temporal configuration model where the nodes temporal activities play the role of the node degrees. We only introduce here the main concepts needed for our purpose, but a full description of the model is given in Appendix A. Importantly, the stationary distribution for walkers coevolving with the network [16] is analytically amenable and provides a natural null model for temporal stability. The stationary walker distribution for a node with activity a is given by

$$\omega_a = \frac{amw+\phi}{a+m\langle a\rangle}, \tag{4}$$

where w is the average density of walkers on a node, ϕ is a scalar that can be obtained numerically in closed form, and $\langle a\rangle$ is the average activity. We use $m=2$ and the activities are computed such that the temporally averaged degree is conserved [15]. Without loss of generality, we can set $w=1/N$, N being the number of nodes in the network, and use Eq. (4) for the stationary walker distribution.

We are now in a position where we can define the temporal stability for a partition $H\{t\}$ of $G\{t\}$ at time scale τ:

$$r_{\tau,\mathscr{H}\{t\}} = \langle \mathrm{Tr}\, R_{t',\tau}[G\{t\},\mathscr{H}\{t\}]\rangle_{t'}, \tag{5}$$

with

$$R_{t',\tau}[G\{t\},\mathscr{H}\{t\}] = \mathbf{H}^T(t')[\Omega\mathcal{M}_G(t',\tau)-\omega^T\omega]\mathbf{H}(t'), \tag{6}$$

where $\Omega=\mathrm{diag}(\omega)$ and the average over t' in Eq. (5) is taken over $[0,T]$ and plays a role similar to the minimum over τ in the static stability. The trace is taken inside the temporal average to allow for partitions of different sizes at different times. Temporal stability is naturally interpreted as the average stability obtained over all windows of size τ for a given temporal partition $\mathscr{H}\{t\}$.

In addition to providing a natural measure to evaluate the relevance of partitions over different time scales τ, temporal stability characterizes the partition $\mathscr{H}^{\mathrm{opt}}[t,\tau]$ with the highest stability for every pair (t,τ). By linearity, the average over t can be unfolded, leaving the expression

$$\mathbf{B}(t,\tau) = [\Omega\mathcal{M}_G(t,\tau)-\omega^T\omega]. \tag{7}$$

The partition $\mathscr{H}^{\mathrm{opt}}[t,\tau]$ optimizing (7) is the same as the one optimizing temporal stability at time t over the time scale τ and can be found by considering Eq. (7) as a modularity optimization problem [17] and solving it with any standard modularity algorithm (e.g., the Louvain method [18]). In Appendix B we give a detailed description of the workflow and provide a link to our code.

III. TWO-BLOCK TOY MODEL

A simple example is useful to illustrate the working of temporal stability and the type of structure it can unveil. Following the model with activity-correlated link classes defined in [19], we consider a toy model network consisting of two blocks of N and N' nodes that follow a simple cycle of temporal interactions repeated M times. Each cycle consists of two interaction windows with a total time period of $T = T_{\mathrm{in}} + T_{\mathrm{out}}$ (see Fig. 1 for an illustration). During the first T_{in} time steps, the nodes only interact within their block with a probability p_{in} per time step; in the remaining T_{out} time steps, the nodes interact exclusively with nodes from the other block with probability p_{out}. Setting $p_{\mathrm{out}} = \frac{T_{\mathrm{in}}p_{\mathrm{in}}}{T_{\mathrm{out}}}\frac{N(N-1)+N'(N'-1)}{2NN'}$ guarantees that the density of links within and between blocks is the same. This makes it impossible to distinguish the two communities at the time-aggregated level.

We then compare the stability of various partitions obtained by aggregating the temporal network over time windows of

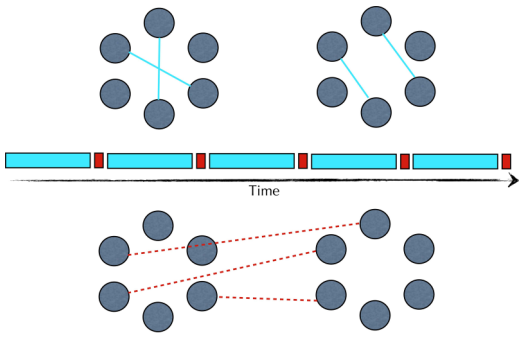

FIG. 1. (Color online) Two-block model. Two blocks of nodes interact following simple alternating rules: During a time window of T_{in} time steps [long (blue) intervals], nodes can create connections only to nodes within their block (top) with probability p_{in}; then during a time window T_{out} [short (red) intervals], they are allowed to interact only with nodes belonging to the other block (bottom) with probability p_{out}. The linking probability for connections within p_{in} and between blocks p_{out} are chosen such as to make the time-aggregated network a single uniform hairball, hiding the temporal nature of the division in two blocks.

[1] While this is not necessary in the case of static stability, because disconnected components can be analyzed separately, it is extremely important for random walkers moving on an evolving network, where such components can drastically change from one slice to the next.

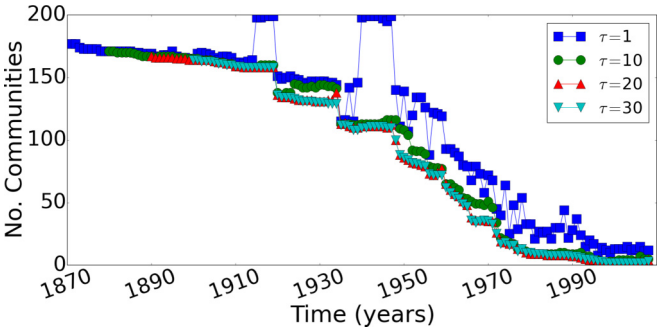

FIG. 2. (Color online) Comparison of the number of communities in optimal partitions for different values of τ in the International Trade Network.

different size $\Delta = 10,20,80$ time steps and the bipartition into the two blocks [Fig. 3(a)]. These partitions represent progressively coarser temporal summaries of the network and we refer to them as Δ partitions. They show how aggregating temporal networks wipes out relevant dynamics. With the simulation setup we used, a crucial value for time is $t = 20$ as it represents the interval of time over which the two blocks are well defined. This is clearly shown by the value of r_τ for the bipartition, which steadily decreases towards zero for $\tau \geqslant T_{\text{in}}$. This illustrates well how temporal stability behaves: The bipartition is a reasonably good approximation over time scales shorter than the mixing cycle, while for longer time scales, the bipartition description is lost in the noise. The parameter τ can then be used to select a time scale over which to compare the relevance of partitions. A partition that is relevant over a short time scale captures essential microdynamics, while at longer time scales other global mechanisms prevail and the microdynamics can be considered as noise. To illustrate this phenomenon we plot in in Fig. 2 the simplest quantity, the number of communities in a partition, for different values of τ in the trade network data set (which we fully introduce in the next section). The shortest time scale $\tau = 1$ yr clearly identifies the World Wars and other events that are precisely located in time. As soon as one switches to a time scale longer than those events, e.g., $\tau = 10$ yr, these effects disappear and the number of communities displays a much smoother behavior over time and captures a different type of dynamics, namely, the densification of links in the network. This effect is even stronger if one considers longer time scales $\tau = 20,30$ yr.

Thus, in our toy model, Δ partitions with $\Delta < T$ perform well for small $\tau < T_{\text{in}}$, as the aggregation window allows for a finer temporal sampling of the network's evolution. Their stability values then continuously decay for growing $\tau \geqslant T_{\text{in}}$ and eventually tend to 0. Moreover, the Δ partitions with $\Delta > T$ perform better for $\tau \geqslant T_{\text{in}}$ as the mixing windows are incorporated in the aggregated networks. Figure 3(a) also display the temporal stability for the optimal partition, found with Eq. (7), which outscores all other partitions for all τ.

The variation of information $v(t,\tau,\tau')$ between $\mathscr{H}^{\text{opt}}[t,\tau]$ and $\mathscr{H}^{\text{opt}}[t,\tau']$ is a useful tool to detect structural changes between clusterings [1,20]. Consider two partitions of a network $\mathscr{X}$ and $\mathscr{Y}$ in k and l communities, respectively.

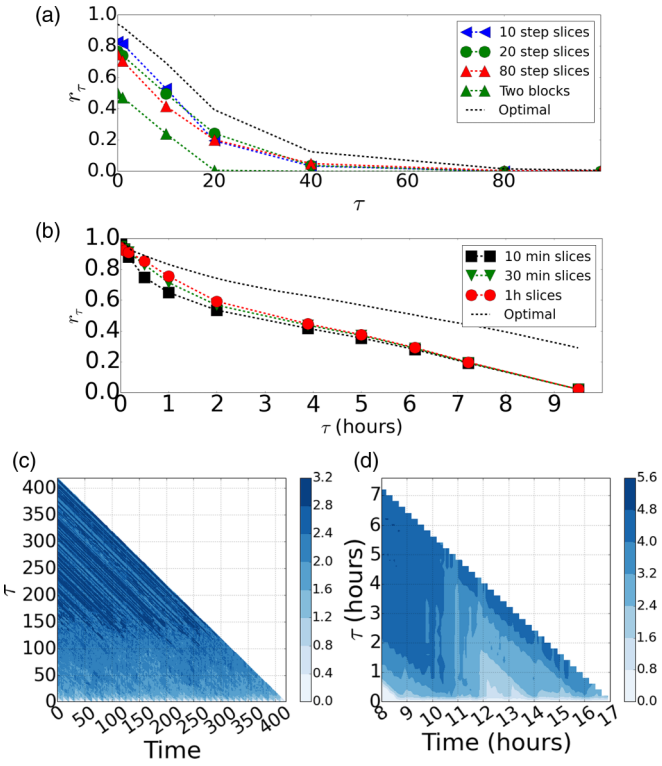

FIG. 3. (Color online) Comparison of the two-block model and SocioPatterns data: temporal stability curves r_τ for the (a) two-block model and (b) SocioPatterns for a selection of Δ partitions against the best temporal clustering obtained from Eq. (7). Temporal stability identifies the periodic nature of the two data sets with the recurring sawtooth pattern evident in the variation from the information $v(t,0,\tau)$ in (c) the two-block model and (d) SocioPatterns. The variation of information is computed from the optimal partitions. The parameters for the two-block model are $N = N' = 10$, $T_{\text{in}} = 20$, $p_{\text{in}} = 0.01$, $T_{\text{out}} = 1$, and $p_{\text{out}} = 0.18$.

Associate with each community in the partition a probability proportional to its cardinality, for example, with $X_i \in \mathscr{X}$ associate $p_i^X = |X_i|/N$, where N is the number of nodes in the network under consideration. Finally, $v(t,\tau,\tau')$ is defined as

$$v(t,\tau,\tau') = H(\mathscr{H}^{\text{opt}}[t,\tau]) + H(\mathscr{H}^{\text{opt}}[t,\tau']) - 2I(\mathscr{H}^{\text{opt}}[t,\tau],\mathscr{H}^{\text{opt}}[t,\tau'], \quad (8)$$

where H is the Shannon entropy and I is the mutual information defined on the probabilities introduced above.

Two special cases are particularly enlightening regarding the evolution of the optimal partition in time: $v(t,0,\tau)$, which informs about the time scale over which structures persist from a time t [see Figs. 3(c) and 4(b)], and $v(t,\tau,\tau+1)$, which gives the instantaneous structural changes between two consecutive time steps $t+\tau$ and $t+\tau+1$ [see Fig. 4(c)], starting at time t. In the first case, key information about stability is given on the ordinate axis and in the second case, sudden changes can be read on the abscissa axis. In the two-block model, information about the state at time t is almost completely lost after two cycles, although this depends on when the initial time t is in the cycle: At the beginning of a cycle a walker is constrained within a block and thus the community structure is stable for a

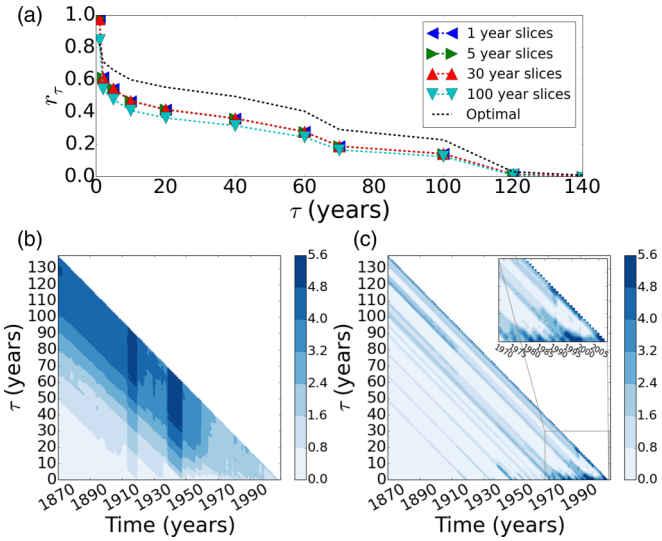

FIG. 4. (Color online) Financial trade network. (a) Temporal stability curves r_τ for different Δ partitions. The optimal temporal clustering is found from an instantaneous temporal slice by temporal stability. Temporal stability confirms (b) the absence of periodicity [variation of information $v(t,0,\tau)$] and (c) regular reorganizations of the community structure of the trade network [variation of information $v(t,\tau,\tau+1)$]. Temporal stability ingeniously identifies abrupt changes in the community structure that correspond to major historical events of the 20th century. The date of said events can be easily read on the abscissa of (b) and (c). The variation of information is computed from the optimal partitions.

longer time; the interblock interaction then comes as a shock for the community structure, producing the sawlike pattern evident in Fig. 3(c). Since the toy model has no additional structure on top of the periodicity, we expect $v(t,\tau,\tau+1)$ to show only noise due to fluctuations in the connectivity within blocks.

IV. REAL DATA SETS

Face-to-face interaction network.. The first real network we analyze is the temporal face-to-face network of children in a primary school described in [21]. The connectivity dynamics of this data set resembles that of the toy model, because children's interactions mostly take place within their class and are punctuated by interclass interactions during breaks and lunch. We repeated the analysis above for one day of contacts and were able to uncover the structures described in [21]. We find that, for short time scales τ, the stability curve obtained for Δ partition with $\Delta = 1h$ has a stability score markedly higher than those of partitions obtained over smaller window sizes [Fig. 3(b)], which potentially contain more information in this τ interval. This reflects the fact that the organization of the children's schedule is organized in hourly periods with short breaks in between. Hence, the dynamics below that time scale does not provide extra information. Like in the toy model, the variation of information $v(t,0,\tau)$ for the optimal partition [Fig. 3(d)] shows that the original information is almost completely lost after 2 h. Since during lunch break children are gathered together and can interact freely across classes, we expect the lunch break to produce a discontinuity. While the temporal stability of the optimal partition is the highest at all delays τ as expected [Fig. 3(b)], $v(t,\tau,\tau+1)$ shows nontrivial patterns that were absent in the toy model example. This indicates that, although the global structure of the children's communities changes slowly in time, it can fluctuate from instant to instant considerably more in comparison to the toy model case, highlighting the presence of the social structures beyond that of the classrooms.

International trade network.. The second real network we consider is the financial trade network over the period 1870–2009 [22,23]. The original data set is weighted and directed. In order to make it consistent with our binary and symmetric null model, we needed to choose a local threshold and forfeit directionality (see Ref. [24] for details). Despite the loss of information due to these simplifications, temporal stability still captures a rich economical phenomenology. As it is conceptually very different from the SocioPatterns data set, we expect to unveil a different type of temporal structure. Indeed, while no periodicity is present, we clearly identify abrupt changes in the community structure between periods of structural stability [Figs. 4(b) and 4(c)]. These structural changes correspond to landmarks of the 20th century's history that had repercussions on the trade network's community structure: For example, two uniform regions are present in Fig. 4(b) between the Great War and the late 1920s and from the late 1920s to the beginning of World War II. Temporal stability therefore identifies the beginning of the Great Depression in 1929. Note also how the regions of uniformity in Figs. 4(b) and 4(c) appear to become shorter proceeding to more recent times and essentially disappear after 1970. It is particularly enlightening to look at Fig. 4(b), which confirms the presence of spells of relative structural calm, interrupted by sudden changes. Zooming in the past 40 years, we also see more frequent localized signatures, which appear to be in connection with notable crisis, including the oil crisis in the 1970s, the speculative bubble of the 1980s, the Gulf War, the fall of the Communist Block, the banking crises of the early 1990s, and finally the 2008 financial crisis.

V. DISCUSSION

To summarize, we introduced temporal stability, a measure related to the modular structure of temporal networks. There are two aspects to temporal stability: First, it enables us to compare the relevance of different time-varying partitions at different time scales and second, it can be used to find the optimal partition over a time scale τ starting at any time t. The main difference between this method and previous ones lies in the conceptually different treatment of the temporal aspect of the problem. Time is naturally embedded in temporal stability as it is based on random walks coevolving with the network. This is in stark contrast with other methods where time is effectively treated as an additional topological constraint and only probed at one time scale. The outcomes of different methods are therefore different and complementary (see Ref. [24] for a comprehensive comparison with multislice modularity). We illustrated the working of temporal stability on different benchmark data sets, showing that it is capable of discerning characteristic time scales of the dynamics

underlying the data sets as well as highlighting single shocks in the systems. As for any target function that includes a comparison between a structure and a notion of randomness, the choice of the null model is crucial. In this article our choice fell on the activity-driven model for two reasons: It constitutes the simplest nontrivial null model and it yields an analytical expression for stationary distribution of random walkers on an evolving network. This in turn allows us to have a closed-form expression for the temporal stability. The equations for temporal stability (5) and (6) can be modified with different null models accounting for different constraints, such as specific temporal behaviors (e.g., temporal correlations), using stationary distributions obtained from simulated ensembles of paths respecting temporal correlations [25], realistic interevent times distributions [26–28], or temporal null models allowing for weighted links. The investigation of the different possible null models is left for future work and is subject to data availability.

ACKNOWLEDGMENTS

The authors acknowledge C. Cattuto and A. Barrat for fruitful discussions and for privileged access to the SocioPatterns data used in this paper. G.P. was supported by the TOPDRIM project funded by the FET program of the European Commission under Contract No. IST-318121.I.D. P.E. was supported by a PET Methodology Program Grant from the MRC UK (Reference No. G1100809/1).

APPENDIX A: ACTIVITY-DRIVEN MODEL DESCRIPTION

The activity-driven network model is a data-driven generator for random temporal networks [15]. In particular, it uses a node's measured activity potential to represent its likeliness to create new links and thus forming its dynamics. Given a network of N nodes, assign to each node i an activity rate a_i, which is the probability per unit time that node i will create a new link to another node. Usually, the activity is given in the form $a_i = \eta x_i$, where x_i is the activity potential. This is done because it allows us to control the average number of active nodes in the network through η. The generation of the network snapshots proceeds as follows.

(i) At time t, start with a network G_t with N disconnected nodes.

(ii) With probability a_i node i creates m links to nodes randomly selected with uniform probability.

(iii) At the following step, remove all edges and iterate.

The simplicity of the model allows us to calculate analytically a number of properties of the resulting network. For example, given a distribution $F(x)$ for the activity potential, the average degree at a given time is given by $\langle k\rangle_t = \frac{2E_t}{N} = 2m\eta\langle x\rangle$ and the degree distribution of the integrated network after T steps for small time and network size is $P_T(k) \sim F[\frac{k}{Tm\eta}]$. More interestingly for our purposes, the activity-driven model allows us to describe the asymptotic distribution of a random walker coevolving with the network [16]. It is in fact possible to write the probability of a random walker to be in node i at time t as

$$P_i(t+\Delta t) = P_i(t)\left[1 - \sum_{j\neq i} \Pi_{i\to j}^{\Delta t}\right] + \sum_{j\neq i} P_j(t)\Pi_{j\to i}^{\Delta t}, \tag{A1}$$

where $\Pi_{i\to j}^{\Delta t}$ is the propagator from i to j over time Δt. In the $\Delta t \to 0$ limit the propagator can be written as $\Pi_{i\to j}^{\Delta t} \sim \frac{\Delta t}{N}(a_i + ma_j)$ and by grouping nodes in activity classes we can write the equation for the probability $W_a(t)$ of finding the walker in a node of activity a at time t as

$$\frac{\partial W_a(t)}{\partial t} = -aW_a(t) + amw - m\langle a\rangle W_a(t) + \int a' W_{a'} F(a')da', \tag{A2}$$

where $w = W/N$ is the density of walkers in the network. Looking for the stationary state of Eq. (A2), one obtains Eq. (4).

APPENDIX B: METHOD WORKFLOW

In this appendix we describe the workflow to follow to obtain the temporal partition with the optimal temporal stability (see Ref. [29]).

(i) Extract the adjacency time series $\{\mathbf{A}_0, \mathbf{A}_1, \ldots, \mathbf{A}_T\}$ of the system.

(ii) Calculate the activity a for each node.

(iii) Calculate ω_a for each class of activity.

(iv) Go through each possible pair $[t,\tau]$ and compute the transition matrix $\mathcal{M}_G(t,\tau)$.

(v) Compute the modularity matrix $\mathbf{B}(t,\tau) = [\Omega\mathcal{M}_G(t,\tau) - \omega^T\omega]$.

(vi) Find the partition $\mathbf{H}^T(t)$ that optimizes $\mathbf{H}^T(t)\mathbf{B}(t,\tau)\mathbf{H}(t)$ using any modularity optimisation algorithm (for example, the Louvain method [18]).

(vii) Finally, average over t to find the temporal stability $r_{\tau,\mathscr{H}\{t\}} = \langle \mathrm{Tr}\, R_{t',\tau}[G\{t\},\mathscr{H}\{t\}]\rangle_{t'}$.

[1] S. Fortunato, Phys. Rep. **486**, 75 (2010).
[2] P. Holme and J. Saramäki, Phys. Rep. **519**, 97 (2012).
[3] P. Mucha, T. Richardson, K. Macon, M. Porter, and J. P. Onnela, Science **328**, 876 (2010).
[4] P. Ronhovde, S. Chakrabarty, D. Hu, M. Sahu, K. K. Sahu, K. F. Kelton, N. A. Mauro, and Z. Nussinov, Eur. Phys. J. E **34**, 105 (2011).
[5] V. Kawadia and S. Sreenivasan, Sci. Rep. **2**, 794 (2012).
[6] Y. Chen, V. Kawadia, and R. Urgaonkar, arXiv:1303.7226v1.
[7] T. G. Kolda and B. W. Bader, SIAM Rev. **51**, 455 (2009).
[8] L. Gauvin, A. Panisson, and C. Cattuto, PLoS ONE **9**, e86028 (2014).
[9] A. Lancichinetti, F. Radicchi, J. J. Ramasco, and S. Fortunato, PLoS ONE **6**, e18961 (2011).

[10] Y. Lin, Y. Zhu, S. Hu, H. Sundaram, and B. L. Tseng, *Proceedings of the 17th International Conference on World Wide Web* (ACM, New York, 2008).
[11] L. Peel and A. Clauset, arXiv:1403.0989.
[12] J. C. Delvenne, S. N. Yaliraki, and M. Barahona, Proc. Natl. Acad. Sci. USA **107**, 12755 (2010).
[13] M. Rosvall and C. T. Bergstrom, PLoS ONE **5**, e8694 (2010).
[14] M. Rosvall, D. Axelsson, and C. Bergstrom, Eur. Phys. J. Spec. Top. **178**, 13 (2009).
[15] N. Perra, B. Gonçalves, R. Pastor-Satorras, and A. Vespignani, Sci. Rep. **2**, 469 (2012).
[16] N. Perra, A. Baronchelli, D. Mocanu, B. Gonçalves, R. Pastor-Satorras, and A. Vespignani, Phys. Rev. Lett. **109**, 238701 (2012).
[17] R. Lambiotte, J.-C. Delvenne, and M. Barahona, arXiv:0812.1770.
[18] V. D. Blondel, J.-L. Guillaume, R. Lambiotte, and E. Lefebvre, J. Stat. Mech. (2008) P10008.
[19] L. Gauvin, A. Panisson, C. Cattuto, and A. Barrat, Sci. Rep. **3**, 3099 (2013).
[20] M. Meilă, Learn. Theor. Kernel Mach. **2777**, 173 (2003).
[21] J. Stehlé, N. Voirin, A. Barrat, C. Cattuto, L. Isella, J.-F. Pinton, M. Quaggiotto, W. Van den Broeck, C. Régis, B. Lina *et al.*, PLoS ONE **6**, e23176 (2011).
[22] K. Barbieri, O. M. Keshk, and B. M. Pollins, Conflict Manag. Peace Sci. **26**, 471 (2009).
[23] K. Barbieri, O. Keshk, and B. Pollins, Correlates of War Project Trade Data Set Codebook, Version 2.0 (2008), available at http://correlatesofwar.org/
[24] See Supplemental Material at http://link.aps.org/supplemental/10.1103/PhysRevE.90.022813 for a detailed description of the data sets and a comprehensive comparison of the method proposed here with the multislice modularity.
[25] A. Barrat, B. Fernandez, K. K. Lin, and L.-S. Young, Phys. Rev. Lett. **110**, 158702 (2013).
[26] L. E. C. Rocha and V. D. Blondel, PLoS Comput. Biol. **9**, e1002974 (2013).
[27] L. E. C. Rocha, F. Liljeros, and P. Holme, PLoS Comput. Biol. **7**, e1001109 (2011).
[28] T. Hoffmann, M. A. Porter, and R. Lambiotte, Phys. Rev. E **86**, 046102 (2012).
[29] The code to perform this is available at https://github.com/lordgrilo/TemporalStability